AFRL-OSR-VA-TR-2014-0291

PLASMONIC ENCODING

Chad Mirkin
NORTHWESTERN UNIVERSITY

10/06/2014
Final Report

Air Force Research Laboratory
AF Office Of Scientific Research (AFOSR)/ RTD
Arlington, Virginia 22203
Air Force Materiel Command

REPORT DOCUMENTATION PAGE

Form Approved
OMB No. 0704-0188

1. REPORT DATE *(DD-MM-YYYY)*	2. REPORT TYPE	3. DATES COVERED *(From - To)*
13-11-2014	Final Performance	01-04-2009 to 30-06-2014

4. TITLE AND SUBTITLE
PLASMONIC ENCODING

5a. CONTRACT NUMBER

5b. GRANT NUMBER
FA9550-09-1-0294

5c. PROGRAM ELEMENT NUMBER

6. AUTHOR(S)
Chad Mirkin

5d. PROJECT NUMBER

5e. TASK NUMBER

5f. WORK UNIT NUMBER

7. PERFORMING ORGANIZATION NAME(S) AND ADDRESS(ES)
NORTHWESTERN UNIVERSITY
633 CLARK ST EVANSTON
EVANSTON, IL 60208-0001 US

8. PERFORMING ORGANIZATION REPORT NUMBER

9. SPONSORING/MONITORING AGENCY NAME(S) AND ADDRESS(ES)
AF Office of Scientific Research
875 N. Randolph St. Room 3112
Arlington, VA 22203

10. SPONSOR/MONITOR'S ACRONYM(S)
AFOSR

11. SPONSOR/MONITOR'S REPORT NUMBER(S)
AFRL-OSR-VA-TR-2014-0291

12. DISTRIBUTION/AVAILABILITY STATEMENT
A DISTRIBUTION UNLIMITED: PB Public Release

13. SUPPLEMENTARY NOTES

14. ABSTRACT
With their small sizes and unique and controllable properties, nanostructures are poised to fulfill an important need in the covert tracking and tagging of materials and living systems. Furthermore, multimodal materials that are able to not only tag, but dramatically affect their environments (e.g. through gene regulation) could be of great interest. To these ends, we proposed two related research paths: the nanowire-based synthesis of novel surface-enhanced Raman scattering (SERS) substrates that are solution dispersible and undetectable by the naked eye called Nanodisk Codes (NDCs), and novel fluorescence-based nanoparticles that can easily transfect cellular membranes and report out on cellular activity, called Nanoflares.

15. SUBJECT TERMS
plasmonic, encoding

16. SECURITY CLASSIFICATION OF:			17. LIMITATION OF ABSTRACT	18. NUMBER OF PAGES	19a. NAME OF RESPONSIBLE PERSON
a. REPORT	b. ABSTRACT	c. THIS PAGE			Chad Mirkin
U	U	U	UU	14	19b. TELEPHONE NUMBER *(Include area code)* 847-467-7302

COVER PAGE
To: technical reports@afosr.af.mil

Subject: Final Progress Report to Dr. Hugh DeLong

Contract/Grant Title: Plasmonic Encoding

Contract/Grant#: FA9550-09-1-0294

Reporting Period: April 1, 2010 to March 31, 2014

Abstract:

With their small sizes and unique and controllable properties, nanostructures are poised to fulfill an important need in the covert tracking and tagging of materials and living systems. Furthermore, multimodal materials that are able to not only tag, but dramatically affect their environments (e.g. through gene regulation) could be of great interest. To these ends, we proposed two related research paths: the nanowire-based synthesis of novel surface-enhanced Raman scattering (SERS) substrates that are solution dispersible and undetectable by the naked eye called Nanodisk Codes (NDCs), and novel fluorescence-based nanoparticles that can easily transfect cellular membranes and report out on cellular activity, called Nanoflares.

In the first year, we improved the performance of existing NDCs by continuing our expansion of the relevant materials palette. We continued to work on Ag nanostructures to make true multicomponent disk code structures and also worked to employ these Ag-based disk codes with multiple excitation wavelengths. This allowed us to broaden the applicability of the already useful NDC system. Additionally, we developed methods to create smaller diameter disk code structures through the on-wire lithography process (OWL) to create even more enhancing substrates.

In years 2 and 3, we further increased the number of unique codes available to Ag NDCs developed in our first funding year by creating code directionality and a system for DNA encryption. In addition, we began studying the unique optical properties of mixed Au and Ag disk ensemble structures that could lead to further increases in NDC functionality. We also extended the work from the first year of funding on smaller diameter on-wire lithography (OWL) structures by optimizing their increased SERS enhancements for future applications in NDCs and chemical and biological detection. Finally, in years 4 and 5, we developed the Nanoflare for use in the active tagging of live cells. These Nanoflares detect, with higher signal-to-noise ratios than previously possible, cellular events in their native environments. Importantly, we used these materials to simultaneously regulate the gene expression of tagged cells. This allows for unprecedented control over cellular environments of interest. Taken together, these advances represent a significant step forward in developing covert tracking and tagging schemes relevant to the Air Force.

OBJECTIVES

Year 1:

1. Confirm previously preliminary results of Ag-based NDC structures through empirical and theoretical methods and extend these studies to encompass multiple excitation wavelengths.
2. Complete initial studies (began last funding period) of Ag-Au systems for multimodal NDC readout.
3. Start development on methods to create narrow diameter (sub-100 nm) OWL nanostructures for eventual development in NDC systems.
4. Develop a new nanoparticle-based system, the Nanoflare, for intracellular detection and tagging.

Year 2:

1. Leverage the nanoflare platform to create a trimodal material that can function as a cellular taggant, biosensor, and gene regulator.
2. Use the unique capabilities of OWL to study the optical properties of mixed Au and Ag disk ensemble structures for potential NDC applications

Year 3:

1. Further extend the number of unique NDC structures for Ag-Au multimodal structures
2. Theoretically and empirically optimize the geometry of sub-100 and sub-50 nm OWL nanostructures for SERS
3. Extend the application of the Nanoflare from detection alone to simultaneous detection and regulation of cell function.

Year 4 and 5– Supplement:

1. Study the fundamental properties of "nanosheets", an important new platform for labeling, tracking, and trace detection.

FINDINGS

There is currently a need for covert tracking and tagging schemes that will allow for advanced reconnaissance and logistics management in the modern world. In previous years of research with the AFOSR, the Mirkin research group has shown how the nanodisk code (NDC) is a novel solution to this challenge. NDCs, which are surface-enhanced Raman scattering (SERS) substrates, consist of functionalized Au nanodisk dimers that are closely spaced and arranged in specific binary patterns. The NDCs were demonstrated to be quite effective at encoding information in multiple ways and were also a powerful biosensing platform. In the last couple of years, we have shown the ability to extend this original work to create Ag NDCs that are more sensitive than their Au counterparts. Additionally, we demonstrated the advantages of shrinking the size of On-Wire Lithography (OWL) dimers for SERS to achieve even higher enhancement factors. Moreover, we developed a new nanosheet material embedding these OWL dimers in a 2D silica-based microscopic scaffold which allows the rational deployment of nanoparticles into complex environments. Recenly, we have worked on using this new platform for labeling, tracking, and trace detection on dollar bills and also studying the mechanical properties of nanosheets prepared using this platform.

We developed a new nanosheet material consisting of micron-sized, ultra-thin, and flexible silica sheets with discrete, highly monodisperse Au nanorod dimers synthesized by OWL. We showed how this solution-dispersible nanosheet material can conform to complex topographies while maintaining the geometry of the nanorod dimers and how they can be used to improve the signal intensity and reproducibility. Additionally, we demonstrated the trace detection of a known marker for illicit drugs on a dollar bill. Another common research area related to paper currency focuses on the development of robust, covert, and easily readable authentication methods for anti-counterfeiting purposes. The nanosheets, like many SERS platforms, are ideally suited for encoding schemes based on the SERS signal from a variety of thiolated small molecules that can serve as specific codes. We then focused on introducing the concept behind the encoding and readout schemes. The nanosheet codes were deposited on dollar bills to test their performance as authentication labels. To do this, a double-blind study was done where each dollar bill was tagged with a unique label using nanosheets on each dollar bill. Tests using a portable Raman spectrometer showed that all of the dollar bills were correctly authenticated. Test results confirm that the nanosheet platform can serve as a new encoding material that could be used easily and reproducibly while being invisible to the naked eye and very difficult to counterfeit. Additionally, we have focused on studying the mechanical properties of silica nanosheet scaffolds using two nanoindentation characterization tools.

In a different type of nanoscale taggant platform, we also demonstrated the concept of the nanoflare. Nanoflares are spherical nucleic acids (SNAs, structures with inorganic nanoparticle

cores and densely-functionalized, highly oriented nucleic acid shells) bound to short, complementary fluorophore-tagged reporter sequences. When bound to the SNA, the fluorophore is in close proximity to the gold nanoparticle, and its fluorescence is quenched. However, in the presence of a longer, target nucleic acid this sequence is displaced from the particle surface, and the fluorescence of the report strand is turned on. This material offers a novel way to alert the presence of a specific chemical or biological target. In the past year, we have made significant progress in the effort to develop this technology into a highly specific therapeutic for genetic disorders, such as cancer. In this way, these structures are capable of regulating aspects of cell function.

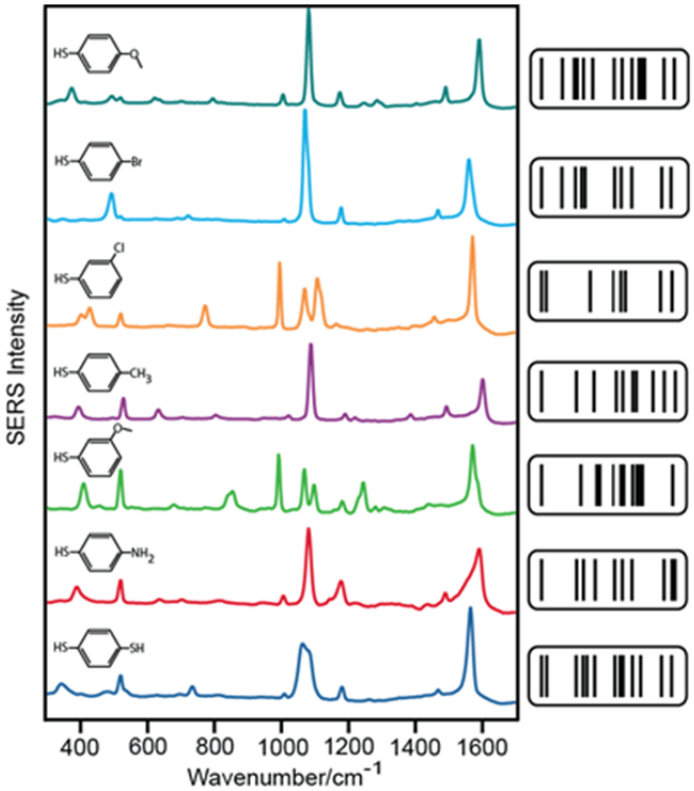

Figure 1. Spectra and corresponding barcodes for all seven of the codes used. From top to bottom, the molecules used are: 4-methoxythiophenol, 4-bromothiophenol, 3-chlorothiophenol, 4-methylthiophenol, 3-methoxythiophenol, 4-aminothiopenol (4-ATP), and 1,4-benzenedithiol (1-4,BDT).

1. Nanosheets In the first year, we developed Ag NDCs that increased the SERS sensitivity of the structures due to the inherent plasmonic advantages of Ag compared to Au. In the second year, we continued along this path by taking advantage of our ability to produce significantly smaller OWL dimers that lead to even larger improvements in their SERS response. During the third year, we took advantage of their inherent ability to be dispersed while maintaining their predesigned geometries to show that the OWL dimers can be used in a variety of detection environments. For example, they can be used in solution-averaged measurements in water and then dropcast on an arbitrary surface to detect molecules adsorbed to that surface. In the fourth year, we worked on the synthesis, characterization, and application of a new silica-based nanosheet material for the delivery of Au dimers to complex environments. These nanosheets effectively harnessed the SERS from individual nanorod dimers and created a collective SERS signal that was macroscopically addressable, reproducible, and strong. We focused on implementing the silica nanosheet platform on a dollar bill to demonstrate its use as a nanoscale barcode that can be easily scanned as a robust, covert, and easily readable authentication method for anti-counterfeiting purposes. The nanosheets, like many SERS platforms, are ideally suited for encoding schemes based on the SERS signal from a variety of thiolated small molecules that can serve as specific codes. By converting the SERS spectrum from a nanosheet into a one-dimensional barcode where

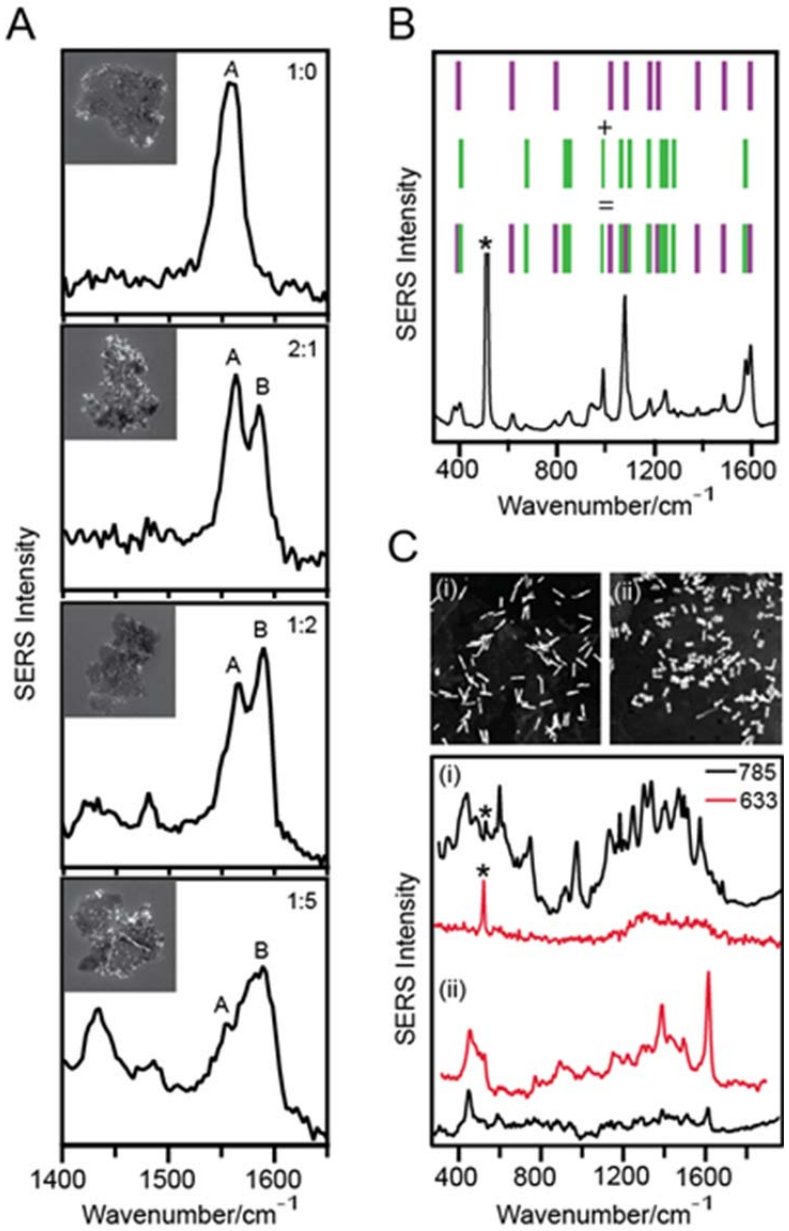

Figure 2. Three different ways to increase the sophistication of the codes by mixing. (A) One sample of nanosheets co-functionalized with two molecules, 1,4-BDT (A) and 4-APT B), where the relative peak heights (A and B, respectively) from each molecule are tailored by controlling their concentrations during functionalization (A:B in top right corner of each spectrum). Inset in each is an SEM image of the single sheet analyzed for the spectra. (B) Two samples of sheets are functionalized separately (4-methylthiophenol and 3-methoxythiophenol in this case) and then mixed in solution and deposited on the surface-of-interest. (C) Two sets of nanosheets are synthesized with one resonant at 785 nm (i) and the other at 633 nm (ii). Each is functionalized with a dye that is resonant at the same wavelength (indocyanine green at 785 nm and methylene blue at 633 nm), and when the codes are mixed and dispensed on a surface, a multimodal code that reads a different spectrum at 785 nm (top) and 633 nm (bottom) results.

the lines correspond to the presence and relative width of the peaks in the spectrum, one can envision an enormous library of potential codes that can be differentiated from one another with a portable Raman spectrometer (the seven unique codes used in this work shown in Figure 1). In addition, the nanosheets are robust and maintain their conformation, while also providing stable signals over long periods of time (months) that can be easily processed into a barcode and analyzed.

Having introduced the concept behind the encoding and readout schemes, the nanosheet codes were deposited on dollar bills to test their performance as authentication labels. To do this, a double-blind study was designed where each dollar bill (out of seventeen total bills) was tagged with a unique label (Figures 1 and 2) by dispensing a very small volume (<1 μL) of a particular nanosheet code over a millimeter-sized area in the same location on each dollar bill (Figure 3A). A portable Raman spectrometer was then used to analyze each dollar bill at this location to test whether it could be correctly matched with the label used for tagging it (Figure 3B). Measured

directly from the dollar bill in the portable Raman spectrometer, a background is observed from the dollar, but the Raman peaks from the labels are clearly observed over this background (Figure 3C, i). After subtracting the background (Figure 3C, ii), the spectrum from each dollar can be converted into a barcode (black lines under the spectra) and can be compared to the library of standard labels for the codes used in this study (Figure 1). In this case, the two standards that matched this particular dollar (serial number beginning with A1893) the closest are compared with the barcode generated from the SERS spectrum, where black lines indicate peaks that are a match between the two and red lines indicate those that are not (Figure 3D). The barcode can easily be identified as 3-cholorothiophenol (left, ~84% match compared to ~52% for 4-methylthiophenol on the right, which was the second closest match). In this same way, each of the other sixteen dollars was also correctly identified with >75% match in every case (Table 1), demonstrating a new encoding material that can be used easily and reproducibly while being invisible to the naked eye and very difficult to counterfeit.

Moreover, we focused on the mechanical properties of the silica nanosheet scaffold. Nanosheets are remarkable due to their flexibility and robustness (Figure 4). The standard fabrication protocol results in synthesis of dispersible nanosheets where many nanorod dimers with well-defined nanogaps are embedded and held at fixed positions relative to one another, creating microscopic and macroscopic entities that avoid issues related to

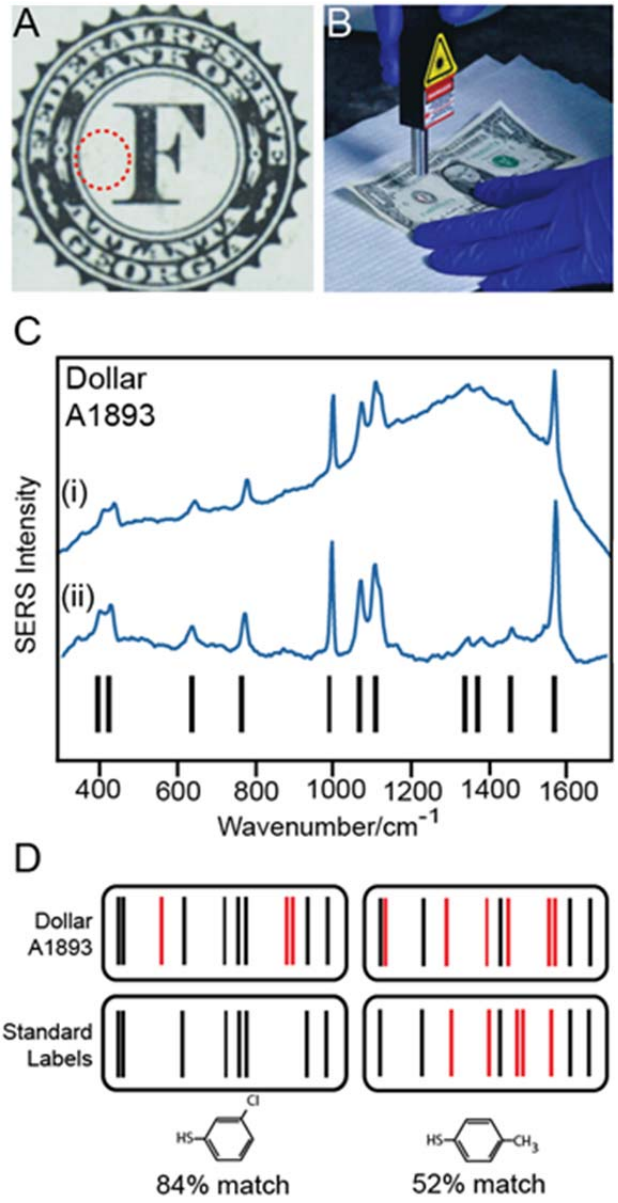

Figure 3. Anti-counterfeiting with nanosheet codes. (A) Photograph of the region where the nanosheets are deposited on each of the seventeen bills used in this double-blind example. (B) Photograph depicting use of the hand-held, portable Raman spectrometer during analysis of the bills. (C) Example spectra before (i) and after (ii) subtracting the background signal for the dollar with the serial number beginning with A1893. The black lines correspond to the presence of peaks and constitute the barcode used for comparison to our standard codes. (D) Examples comparing the code generated in (C) to the two closest matches (3-chlorothiophenol on the left and 4-methylthiophenol on the right), where black lines indicate a match between the two and red lines indicate a peak that is only present in one. The bill is positively matched to 3-chlorothiophenol in this case (~84% match), demonstrating successful analysis of the code.

aggregation of the nanowires. The sheets could cover a number of other complex surfaces, including discrete bacteria cells deposited on a surface (*e.g. Escherichia coli*), micron-sized spheres, and random surface topography (Figure 4). In all cases, the nanosheets conformed to the morphology of the samples, effectively wrapping around them and positioning the nanorods in proximity to their highly convex surfaces.

Dollar Serial #	Dollar Label	Dollar Year	Predicted Molecule	% Match	Correct Molecule
K18265188	B	2006	4-MBT	91	4-MBT
J69943198A	E	2006	3-Methoxy	78	3-Methoxy
K63443108D	F	2006	1,4-BDT	89	1,4-BDT
F56672285B	G	2006	3-Methoxy	83	3-Methoxy
L81982245H	H	2009	4-Bromo + 4-Meth	85	4-Bromo + 4-Meth
A18937143A	I	2006	3-Chloro	81	3-Chloro
G30475445C	L	2006	3-Chloro	77	3-Chloro
K38509828A	M	2009	4-APT	85	4-APT
D67062729D	N	2006	4-Bromo	92	4-Bromo
K22774856B	Q	2009	4-Meth	87	4-Meth
B62039428A	R	2009	blank	84	blank
B08185711A	U	2009	4-APT	77	4-APT
B90201261C	V	2009	1,4-BDT	94	1,4-BDT

Table 1. Results from double-blind dollar authentication study. Predicted molecule is the standard code that was paired with experimental spectrum from each dollar, and percent match is the percentage of the peaks that matched between the two. Correct molecule is the nanosheet code that was actually applied to the dollars. "Blank" corresponds to unfunctionalized nanosheets without a molecule present to serve as a control.

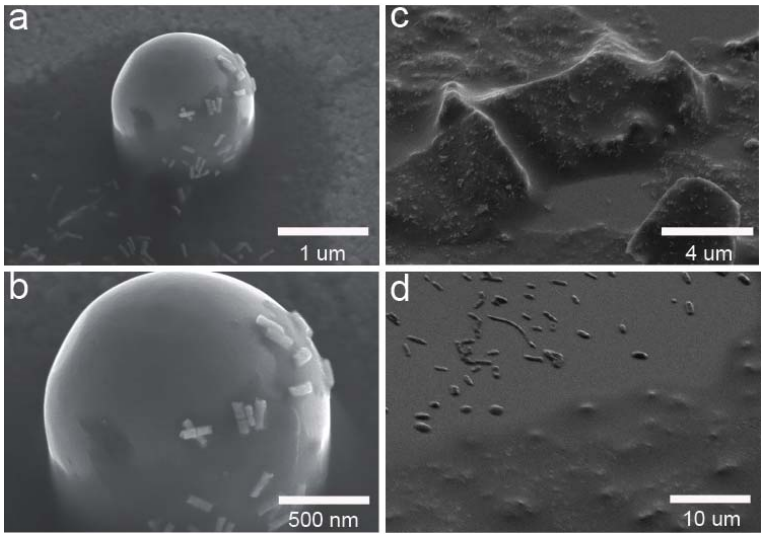

Figure 4. SEM images of the nanosheets deposited on a number of complex topographies. (A,B) Images of the wrapping around and adhering to a micron-sized silica sphere. (C) A group of nanosheets conforming to complex, random debris on a silicon wafer. (D) Nanosheets covering a group of Escherichia coli cells, where the boundary of covered and uncovered cells is visible.

We used nanoindentation techniques with the aid of a high precision atomic force microscope (AFM) to study the mechanical properties of these silica sheets. The mechanical properties were probed by indenting (loading/unloading) at the center of an isolated nanosheet on a silicon wafer. We used high spring constant probes (from Bruker Corporation) for mechanical testing. Two sets of measurements were done, first with quantitative nanomechanical property mapping (peak force QNM) which gives very accurate and surface sensitive measurements for thin films (Figure 5A-C). Indentation was performed at numerous locations and depths on the sample to minimize substrate effects. The modulus map of a silica sheets were plotted and average Young's modulus values were measured to be ~1.1 to 1.8 GPa depending on the thickness. Similarly, the hardness values were measured to be ~58 to 80 MPa for silica nanosheet samples. Secondly, we performed the mechanical characterization with feedback based displacement control method using a Hysitron

Triboindenter characterization tool. Measurements results were consistent with the results obtained using peak force QNM setup (Figure 5D). In both cases, measured values were very small compared to the standard samples. Moreover, we observed a slight rise in the hardness strength with increase in nanosheet thickness. This further understanding of the mechanical properties will used to optimize and tailor the fabrication conditions for deployment of nanosheets in specific environments (like the surface of human hair).

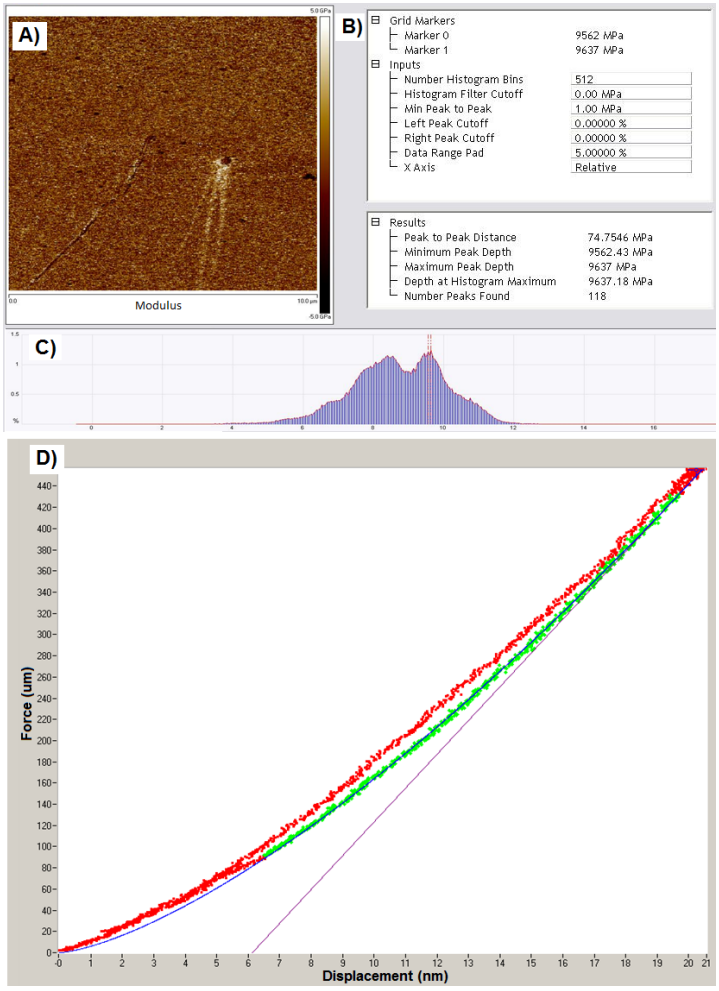

Figure 5. Mechanical characterization of silica nanosheets. (A) Young's modulus map of the nanosheet plotted using an atomic foce microscope (peak force QNM), (B) corresponding characterization results for the region of interest, (C) distribution of Young's modulus values over the scanned surface. (D) Force-displacement plots which were acquired with feedback based displacement method using a Hysitron Triboindenter characterization tool.

2. Nanoflares In 2007, we first introduced the concept of nanoflares. Nanoflares are a new class of spherical nucleic acid (SNA)-based probes that are comprised of a densely functionalized oligonucleotide shell and an inorganic nanoparticle core. The oligonucleotide capture sequence attached to the nanoparticle hybridizes with short, fluorophore-labeled DNA molecules, termed "flares". In this conformation, the close proximity of the fluorophore to the Au NP surface leads to quenching of the fluorescence. However, when a target mRNA binds to the capture sequence, the concomitant displacement of the flare can be detected as a corresponding increase in fluorescence (Figure 6). The ability of these nanoconjugates to both bind to specific genetic targets and identify that binding event with the release of a fluorophore has allowed the nanoflare to be used as both an efficient anti-sense regulator of gene expression and an extremely sensitive diagnostic of disorders with a genetic basis.

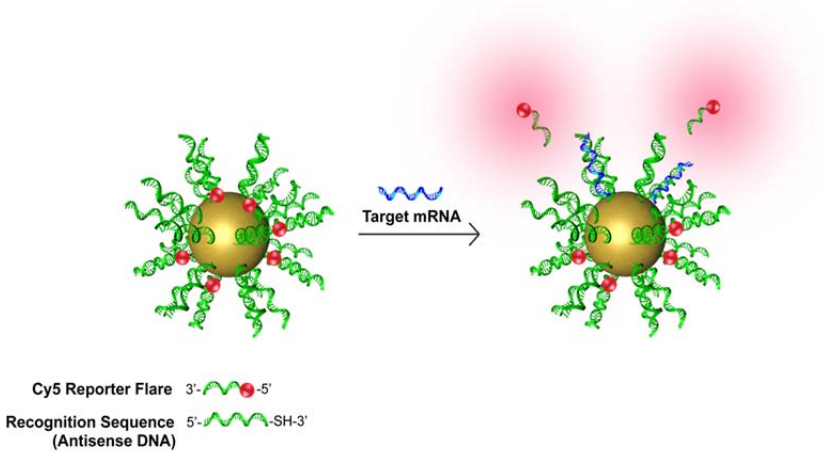

Figure 6: Schematic of Nanoflare target recognition and binding

We have worked on expanding the capability of the nanoflare into a construct that can both quantify RNA expression in live cells, and also report the specific location of target transcripts within the cell.The localization of mRNA has emerged as an essential process for restricting certain proteins to specific, often asymmetrical compartments within cells. For instance synaptic potentiation, the basis of learning and memory, relies upon the local translation of specific mRNAs in pre- and post-synaptic compartments. Likewise, the misregulation of mRNA distribution is associated with a number of disorders, including mental retardation syndrome and cancer metastasis. However, despite the significant role of mRNA localization in cellular function, to date there are no effective methods to visualize this phenomenon in live cells. We have developed such a method based on the NanoFlare architecture previously reported in the Mirkin group. These highly negatively charged nanostructures do not require cationic transfection agents or additional particle surface modifications and naturally enter all cell lines tested to date (over 50, including primary cells) in high quantities. Further, they exhibit enhanced target hybridization, resistance to enzymatic breakdown and low immune response compared to free nucleic acids. Together, these properties make the Nanoflare an ideal platform for studying dynamic intracellular processes. To this end we have developed a Nanoflare-like construct, referred to as the StickyFlare, which utilizes antisense flares capable of binding to and traveling with mRNA targets (Figure 7). This construct maintains the ability of the Nanoflare to quantify RNA expression in live cells, and adds the ability to observe dynamically the transport and localization of targeted transcripts. We have used this new nanoconjugate to probe the intracellular localization of β–actin mRNA in live cells, including cervical cancer HeLa cells, and mouse embryonic fibroblasts (MEFs). Interestingly, the intracellular localization of the same transcript in these two cell types is starkly different. In HeLas β–actin mRNA colocalizes with mitochondria, whereas in MEFs the mRNA is transported to the growth cones of dendritic outgrowths, where it undergoes local translation to drive cell growth and motility (Figure 8). Importantly, these are not static analyses, but maintained real-time imaging that can be combined into a movie to show the dynamics of β–actin transport within each cell. To our knowledge this construct is the first analytical tool capable of giving such a complete report of RNA function, that is to

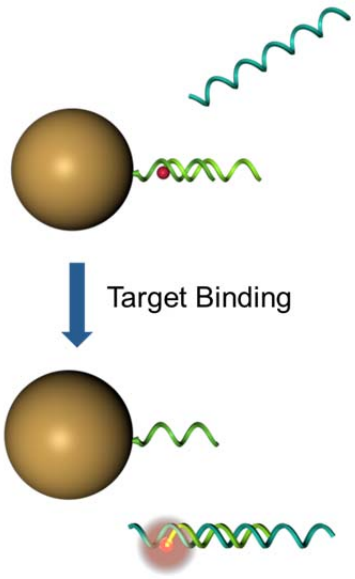

Figure 7: Schematic of Stickyflare target recognition and binding

simultaneously report RNA concentration and spatial localization in live cells.

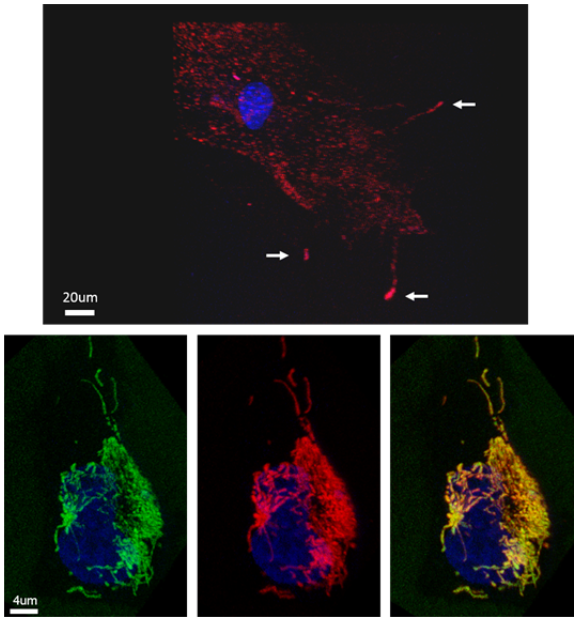

Figure 8: StickyFlare shows mRNA localization in live cells. Upper panel: β–actin mRNA is transporter to the growth cone of dendritic outgrowths (white arrows). Lower panels: β–actin SFs colocalize with mitochondria in HeLa cells. Left, mitochondrial stain; middle, β–actin SF; right, overlay showing colocalization.

SUPPORTED PERSONNEL

Chad Mirkin (Professor)
Matthew Rycenga (Postdoctoral Fellow)
Gilles Bourret (Postdoctoral Fellow)
Xiaozhu Zhou (Postdoctoral Fellow)
Bryan Mangelson (Graduate Student)
Kyle Osberg (Graduate Student)
Michelle Personick (Graduate Student)
Alejo Lifschitz (Graduate Student)
Abrin Schmucker (Graduate Student)
Soyoung Seo (Graduate Student)
Mark Langille (Graduate Student)
Daniel Park (Graduate Student)
Matt Jones (Graduate Student)
Jose Mendez-Arroyo (Graduate Student)

COLLABORATIONS

- X-ray scattering work was completed in collaboration with Dr. Byeongdu Lee at the Argonne National Lab Advanced Photon Source

- Theoretical work was performed in collaboration with Prof. George Schatz (Northwestern) and his group
- Experimental work was performed in collaboration with Profs. Hua Zhang and Freddy Boey (Nanyang Technological University) – students were exchanged

PUBLICATIONS

1. Xu, X.; Daniel, W. L.; Wei, W.; Mirkin, C. A. "Colorimetric Cu^{2+} Detection Using DNA Modified Gold Nanoparticle Aggregates as Probes and Click Chemistry," *Small* **2010**, *6*, 623-626.
2. Macfarlane, R. J.; Jones, M. R.; Senesi, A. J.; Young, K. L.; Lee, B. Y.; Wu, J.; Mirkin, C. A. "Establishing the Design Rules for DNA-Mediated Programmable Colloidal Crystallization," *Angew. Chem.,* **2010**, *49*, 4589-4592.
3. Li, S.; Pedano, M.; Chang, S.-H.; Mirkin, C. A.; Schatz, G. C. "Gap structure effects on SERS intensities for gold gapped-rods," *Nano Letters*, **2010**, *10*, 1722-1727.
4. Jones, M. R.; Macfarlane, R. J.; Lee, B.; Zhang, J.; Young, K. L.; Senesi, A. J.; Mirkin, C. A. "DNA-Nanoparticle Superlattices Formed From Anisotropic Building Blocks," *Nature Materials*, **2010**, *9*, 913-917.
5. Banholzer, M. J.; Osberg, K. D.; Li, S.; Mangelson, B. F.; Schatz, G. C.; and Mirkin, C. A. "Silver-based Nanodisk Codes," *ACS Nano*, **2010**, *9*, 5446-5452.
6. Zhang, J.; Langille, M. R.; Personick, M. L. ; Zhang, K. ; Li, S. ; Mirkin, C. A. "Concave Cubic Gold Nanocrystals with High-Index Facets," *J. Am. Chem. Soc.*, **2010**, *132*, 14012–14014.
7. Schmucker, A. L.; Harris, N.; Banholzer, M. J.; Blaber, M. G.; Osberg, K. D.; Schatz, G. C.; Mirkin, C. A. "Correlating Nanorod Structure With Experimentally Measured and Theoretically Predicted Surface Plasmon Resonance," *ACS Nano*, **2010**, *9*, 5453-5463.
8. Liusman, C.; Li, S.; Chen, X.; Wei, W. D.; Zhang, H.; Schatz, G.; Boey, F.; Mirkin, C. A. "Free Standing Bimetallic Nanorings and Nanoring Arrays Made by On-Wire Lithography (OWL)," *ACS Nano*, **2010**, *4*, 7676-7682.
9. Mirkin, C. A. "The Polyvalent Gold Nanoparticle Conjugate-Materials Synthesis, Biodiagnostics, and Intracellular Gene Regulation," *MRS Bulletin*, **2010**, *35*, 532-539.
10. Osberg, K. D.; Schmucker, A. L.; Senesi, A. J.; Mirkin, C. A. "One-Dimensional Nanorod Arrays: Independent Control of Composition, Length, and Interparticle Spacing with nanometer Precision," *Nano Letters*, **2011**, *11*, 820–824.
11. Jones, M. R.; Macfarlane, R. J.; Prigodich, A. E.; Patel, P. C.; Mirkin, C. A. "Nanoparticle Shape Anisotropy Dictates the Collective Behavior of Surface-Bound Ligands," *J. Am. Chem. Soc*., **2011**, *133*, 18865-18869.
12. Patel, P.; Hao, L.; AuYeung, W. S.; Mirkin, C. A. "Duplex End Breathing Determines Serum Stability and Intracellular Potency of siRNA-Au NPs," *Molecular Pharmaceutics*, **2011**, *8*, 1285-1291.
13. Huang, X.; Li, S. Z.; Huang, Y. Z.; Wu, S. X.; Zhou, X. Z.; Li, S. Z.; Gan, C. L.; Boey, F.; Mirkin, C. A.; Zhang, H. "Synthesis of Hexagonal Close-Packed Gold Nanostructures," *Nature Commun*., **2011**, *2*, 292.

14. Auyeung, E.; Cutler, J. I.; Macfarlane, R. J.; Jones, M. R.; Zhang, K.; Mirkin, C. A. "Synthetically Programmable Nanoparticle Superlattices Using a Hollow Three-Dimensional Spacer Approach," *Nature Nanotech.*, **2011**, *7*, 24-28.
15. Hao, L.; Patel, P.; Alhasan, A.; Giljohann, D.; Mirkin, C. "Nucleic Acid-Gold Nanoparticle Conjugates as Mimics of microRNA," *Small*, **2011**, *7*, 3158-3162.
16. Cutler, J. I.; Auyeung, E.; Mirkin, C. A. "Spherical Nucleic Acids," *J. Am. Chem. Soc.*, **2012**, *134*, 1376–1391.
17. Imahori, H.; Kitaura, S.; Kira, A.; Hayashi, H.; Nishi, M.; Hirao, K.; Zhe, Z.; Miyato, Y.; Noda, K.; Matsushige, K.; Tkachenko, N. V.; Lemmetyinen, H.; Qin, L.; Hurst, S. J.; Mirkin, C. A. "A Photoconductive, Thiophene-Fullerene Copolymer, Bulk Hetero-Junction Nanorod Device," *J. Phys. Chem. Lett.*, **2012**, *3*, 478-481.
18. Ringe, E.; Zhang, J.; Langille, M. R.; Mirkin, C. A.; Marks, L. D.; Van Duyne, R. P. "Correlating the Structure and Localized Surface Plasmon Resonance of Single Silver Right Bipyramids," *Nanotechnology*, **2012**, *23*, 444005.
19. Ringe, E.; Langille, M. R.; Sohn, K.; Zhang, J.; Huang, J.; Mirkin, C. A.; Van Duyne, R. P.; Marks, L. D. "Plasmon Length: A Universal Parameter to Describe Size Effects in Gold Nanoparticles," *J. Phys. Chem. Lett.*, **2012**, *3*, 1479–1483.
20. Osberg, K.; Rycenga, M.; Harris, N.; Schmucker, A. L.; Langille, M.; Schatz, G. C.; Mirkin, C. A. "Dispersible Gold Nanorod Dimers with Sub-5 nm Gaps as Local Amplifiers for Surface-Enhanced Raman Scattering," *Nano Lett.*, **2012**, *12*, 3828–3832.
21. Langille, M. R.; Personick, M. L; Zhang, J.; Mirkin, C. A. "Defining the Rules for the Shape Evolution of Gold Nanoparticles," *J. Am. Chem. Soc.*, **2012**, *134*, 14542–14554.
22. Auyeung, E.; Macfarlane, R. J.; Choi, C. H. J.; Cutler, J. I.; Mirkin, C. A. "Transitioning DNA-Engineered Nanoparticle Superlattices from Solution to the Solid State," *Adv. Mater.*, **2012**, *24*, 5181-5186.
23. Zhou, X.; Shade, C. M.; Schmucker, A. L.; Brown, K. A.; He, S.; Boey, F. Y. C.; Ma, J.; Zhang, H.; Mirkin, C. A. "OWL-Based Nanomasks for Preparing Graphene Ribbons with Sub-10 nm Gaps," *Nano Lett.*, **2012**, *12*, 4734–4737.
24. Osberg, K. D.; Rycenga, M. J.; Bourret, G. R.; Brown, K. A.; Mirkin, C. A. "Dispersible Surface-Enhanced Raman Scattering Nanosheets," *Adv. Mater.*, **2012**, *24*, 6065–6070.
25. Rycenga, M.; Langille, M. R.; Personick, M. L.; Ozel, T.; Mirkin, C. A. "Chemically Isolating Hot Spots on Concave Nanocubes," *Nano Lett.*, **2012**, *12*, 6218–6222.
26. Langille, M. R.; Zheng, J.; Personick, M. L.; Mirkin, C. A. "Stepwise Evolution of Spherical Seeds into 20-Fold Twinned Icosahedra," *Science*, **2012**, *337*, 954-957.
27. Personick, M. L.; Langille, M. R.; Zhang, J.; Wu, J.; Li, S.; Mirkin, C. A. "Plasmon-Mediated Synthesis of Silver Cubes with Unusual Twinning Structures Using Short Wavelength Excitation," *Small*, **2013**, *9*, 1947-1953.
28. Personick, M. L.; Langille, M. R.; Wu, J.; Mirkin, C. A. "Synthesis of Hexagonal Gold Bipyramids Directed by Planar-Twinned Silver Triangular Nanoprisms," *J. Am. Chem. Soc.*, **2013**, *135*, 3800-3803.
29. Jones, M. R.; Mirkin, C. A. "Bypassing the Limitations of Classical Chemical Purification with DNA-Programmable Nanoparticle Recrystallization," *Angew. Chem.*, **2013**, *52*, 2886-2891.
30. Bourret, G. R.; Ozel, T.; Blaber, M.; Shade, C. M.; Schatz, G. C.; Mirkin, C. A. "Long-Range Plasmophore Rulers," *Nano Lett.*, **2013**, *13*, 2270-2275.

31. Zhou, X.; He, S; Brown, K. A.; Arroyo, J.; Boey, F.; Mirkin, C. A. "Locally Altering the Electronic Properties of Graphene By Nanoscopically Doping It With Rhodamine 6G," *Nano Lett.*, **2013**, *13*, 1616–1621.
32. Macfarlane, R. J.; O'Brien, M. N; Petrosko, S. H.; Mirkin, C. A. "Nucleic Acid-Modified Nanostructures as Programmable Atom Equivalents: Forging a New Periodic Table," *Angew. Chem.*, **2013**, *52*, 5688-5698.
33. Mangelson, B. F.; Park, D. J.; Ku, J. C.; Osberg, K. D.; Schatz, G. C.; Mirkin, C. A. "Tunable and Broadband Plasmonic Absorption via Dispersible Nanoantennas with Sub-10 nm Gaps," *Small*, **2013**, 9, 2250-2254.
34. Zhang, C.; Macfarlane, R. J.; Young, K. L.; Choi, C. H. J.; Hao, L.; Auyeung, E.; Liu, G. Zhou, X.; Mirkin, C. A. "A General Approach to DNA-Programmable Atom Equivalents," *Nature Mater.*, **2013**, 12, 741-746.
35. Langille, M. R.; Personick, M. L.; Mirkin, C. A. "Plasmon-Mediated Syntheses of Metallic Nanostructures," *Angew. Chem.*, **2013**, 52, 13910-13940.
36. Ozel, T.; Bourret, G. R.; Schmucker, A. L.; Brown, K. A.; Mirkin, C. A. "Hybrid Semiconductor Core-Shell Nanowires with Tunable Plasmonic Nanoantennas," *Adv. Mater.*, **2013**, 25, 4515-4520.
37. Senesi, A. J.; Eichelsdoerfer, D. J.; Macfarlane, R. J.; Jones, M. R.; Auyeung, E.; Lee, B.; Mirkin, C. A. "Stepwise evolution of programmable DNA-nanoparticle superlattices," *Angew. Chem.*, **2013**, 52, 6624-6628.
38. Macfarlane, R. J.; Jones, M. R.; Lee, B.; Auyeung, E.; Mirkin, C. A. "Topotactic Interconversion of Nanoparticle Superlattices," *Science*, **2013**, 341, 1222-1225.
39. Walter, S. R.; Young, K. L.; Holland, J. G.; Gieseck, R. L.; Mirkin, C. A.; Geiger, F. M. "Counting the Number of Magnesium Ions Bound to The Surface-immobilized Thymine Oligonucleotides That Comprise Spherical Nucleic Acids," *J. Am. Chem. Soc.,* **2013**, 135, 17339-17348.
40. Liu, G.; Young, K.L.; Liao, X.; Personick, M.L.; Mirkin, C.A. "Anisotropic Nanoparticles as Shape-Directing Catalysts for the Chemical Etching of Silicon" *J. Am. Chem. Soc.,* **2013**, 135, 12196-12199.
41. Young, K. Y.; Ross, M. B.; Blaber, M. G.; Rycenga, M. J.; Jones, M. R.; Zhang, C.; Senesi, A. J.; Lee, B.; Schatz, G. C.; Mirkin, C. A. "Using DNA to Design Plasmonic Metamaterials with Tunable Optical Properties," *Adv. Mater.*, **2014**, 26, 653-659.
42. Personick, M.; Mirkin, C. A. "Making Sense of the Mayham Behind Shape Control in the Synthesis of Gold Nanoparticles," *J. Am. Chem. Soc.*, **2013**, 135, 18238-18247.
43. Schmucker, A. L., Dickerson, M. B., Rycenga, M., Mangelson, B. F., Brown, K. A., Naik, R. R., Mirkin, C. A. "Combined Chemical and Physical Encoding with Silk Fibroin-Embedded Nanostructures," *Small*, **2014**, 10, 1485-1489
44. Zhou, X.; Zhou, Y.; Ku, J.; Zhang, C.; Mirkin, C. A. "Capillary Force-driven, Large-area Alignment of Multi-segmented Nanowires," *ACS Nano*, **2014**, 8, 1511-1516
45. O'Brien, M. N.; Jones, M. R.; Brown, K. A.; Mirkin, C. A. "Universal Noble Metal Nanoparticle Seeds Realized Through Iterative Reductive Growth and Oxidative Dissolution Reactions," *J. Am. Chem. Soc.,* **2014**, 136, 7603-7606
46. Zhou, Y.; Zhou, X.; Park, D.; Torabi, K.; Brown, K.; Jones, M. R.; Zhang, C.; Schatz, G. C.; Mirkin, C. A. "Shape-Selective Deposition and Assembly of Anisotropic Nanoparticles," *Nano Letters*, **2014**, 14, 2157-2161.

47. Radha, B.; Senesi, A.J.; O'Brien, M. N.; Wang, M.; Auyeung, E.; Lee, B.; Mirkin, C. A.; "Reconstitutable Nanoparticle Superlattices," *Nano Letters*, **2014**, 14, 2162-2167.

INTERACTIONS/TRANSITIONS

1. Functionalization of Anisotropic Nanostructures, Matthew R Jones, Robert J Macfarlane, Chad A. Mirkin, Andrew J Senesi, Kaylie L Young, Jian Zhang, 61/367,142.
2. Dispersible Nanoparticle-Embedded Nanosheets, Chad A. Mirkin, Keith A. Brown, Kyle D. Osberg, Matthew J. Rycenga, Gilles Bourret, 61/677,810;PCT/US2013/052610.
3. Broadband Plasmonic Absorber with Hotspot Generating Gapped Nanoantenna, Chad A. Mirkin, George C. Schatz, Bryan F. Mangelson, 61/722,319.
4. Coaxial Lithography, Chad A. Mirkin, Gilles R. Bourret, Tuncay Ozel, 61/981,921;62/000,861.
5. Synthesis of Uniform Gold Nanoparticles through Reductive Growth and Oxidative Dissolution Reactions, Matthew R Jones, Chad A. Mirkin, Matthew O'Brien, 62/023,398.